Journal of Process Control xxx (2010) xxx–xxx

Contents lists available at ScienceDirect

Journal of Process Control

journal homepage: www.elsevier.com/locate/jprocont

Instabilities and multiplicities in non-isothermal blown film extrusion including the effects of crystallization

J. Carl Pirkle Jr.[a], Richard D. Braatz[b,*]

[a] University of Illinois at Urbana-Champaign, 600 South Mathews Avenue, Urbana, IL 61801, United States
[b] Massachusetts Institute of Technology, Department of Chemical Engineering, Room 66-372, 77 Massachusetts Avenue, Cambridge, MA 02139, United States

ARTICLE INFO

Article history:
Received 25 February 2010
Received in revised form
15 December 2010
Accepted 17 December 2010
Available online xxx

Keywords:
Distributed parameter systems
Differential-algebraic equations
Nonlinear dynamics
Stability analysis
Polymer processes
Polymer film extrusion

ABSTRACT

Stable operating regions for blown film extrusion are mapped using a dynamic model that includes the effect of crystallization on the rheological properties of the polymer. In the computations, the bubble air mass and take-up ratio were held constant, and the machine tension and bubble inflation pressure were treated as dependent variables. For a given bubble air mass, the take-up ratio was used as the continuation parameter for mapping steady-state solutions. The take-up ratio varies smoothly, but not necessarily monotonically, with the machine tension. Curves of either blow-up ratio or thickness reduction versus take-up ratio reveal that there are take-up ratios where no, one, or multiple solutions exist. The heat transfer coefficient from the polymer film to the external air and surroundings has a marked influence on the qualitative and quantitative features of the blow-up ratio versus thickness reduction curves. Generalized eigenvalue analysis of the linearized blown film equations indicates that increasing the heat transfer rate increases the stability of operations. A corresponding decline occurs, however, in the thickness reduction of the blown film for a given blow-up ratio.

1. Introduction

Blown film extrusion is a widespread commercial process for the manufacture of plastic sheets, shrink-wrap, and many useful household items such as garbage bags, plastic wrap, sandwich bags, food storage bags, sausage casings. Blown film extrusion has many advantages for the commercial production of polymeric films and sheets. Biaxial stretching of the molten polymer during extrusion produces plastic film that is superior to uniaxial flat-sheet extrusion. The biaxial stretching effects on molecular orientation, conformation, and crystallization result in a higher strength thin plastic film.

In blown film extrusion, molten polymer is extruded through an annular die while air is fed through an inner concentric bubble-tube (see Fig. 1). This internal air causes the cylindrical film to inflate, increasing the radius of the polymer bubble by stretching it in two directions, and decreasing the film thickness. Simultaneously, the guide rolls above the die flatten the film, and the nip rolls subject the film to tension in the axial (upward from the die) direction. The sum of the tensions provided by the nip rolls and the axial component of the bubble inflation force is called the machine tension. External air supplied from a concentric outer ring cools the film. The resulting temperature reduction increases the viscosity of the rising film and eventually induces crystallization as the temperature drops below the melting point of the polymer. The crystallization, in turn, causes an additional increase in viscosity, and the polymer solidifies.

The solidification zone is called the freeze zone or frost zone [1]. Within this region, the rapidly increasing viscous stiffness causes the bubble radius and the film thickness to stabilize, changing very little as the film heads upward toward the nip rolls. The position within the freeze zone at which the bubble radius change is imperceptible is called the frost line. The nip rolls and the bubble inflation combine to create an elongating force on the polymer bubble-tube and the inflating air causes a circumferential tension on the bubble-tube. The resulting biaxial stress can induce further crystallization, an action termed flow-induced crystallization. Although this effect has been included in recent work involving microstructural constitutive relations [2–7], it is neglected in earlier models of blown film extrusion [8–10].

Several linearized stability analyses have been applied to the film blowing process, beginning with Yeow [11], who derived the dynamic equations and analyzed an isothermal Newtonian fluid. This was followed by Cain and Denn [8] for both Newtonian and viscoelastic constitutive relationships such as the upper convected Maxwell and Marrucci models. Both viscoelasticity and film cooling had stabilizing influences. Also, holding the bubble air mass and nip-roll speed constant increased the stability zone over that arising from constraining bubble inflation pressure and nip-roll

* Corresponding author. Tel.: +1 617 253 3112; fax: +1 617 258 0546.
E-mail address: braatz@mit.edu (R.D. Braatz).

0959-1524/$ – see front matter © 2010 Elsevier Ltd. All rights reserved.
doi:10.1016/j.jprocont.2010.12.007

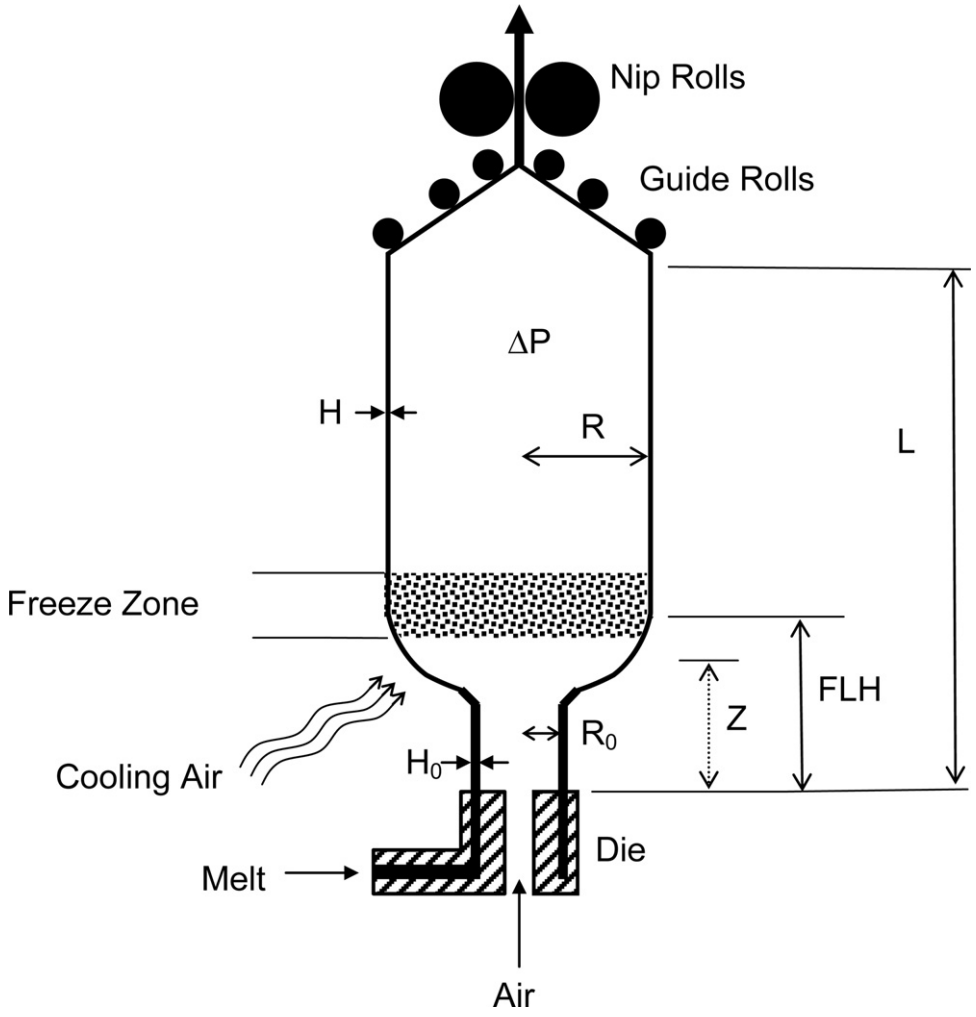

Fig. 1. Blown film extrusion.

speed. This finding was confirmed in later studies by Yoon and Park [10,12], who applied their analysis to two-layer blown film extrusion. Later studies, in which bubble air mass and nip-roll speed were held constant, examined conditions leading to the onset of draw-resonance and helical instabilities [13–15]. None of these investigations included the effect of crystallization on stability.

Crystallization was considered by Pirkle and Braatz [16], who conducted a rather limited stability study for the non-isothermal thin-shell model of blown film extrusion using a quasi-Newtonian stress-thinning constitutive relation for low-density polyethylene (LDPE). The dimensionless bubble inflation pressure force B_1 and modified machine tension parameter F were held constant, which are related to the total tension T_Z in the machine direction by $T_Z = B_1 r_L^2 + F$, where r_L is the blowup ratio. With B_1 and all other operating conditions held constant, varying F enabled the speedy calculation of blow-up ratio, thickness reduction, and take-up ratio. For the limited range of simulated conditions that were investigated, no discontinuities in the blow-up ratio, thickness reduction, or take-up ratio were observed. A stability study by Henrichsen and McHugh [6] included crystallization, albeit while using an approximation to the momentum equations. They did not constrain bubble air mass and nip-roll speed in their analysis.

For computer simulation, either (i) air bubble inflation pressure and modified machine tension [16] or (ii) bubble air mass and nip-roll speed [7] can be set as constants. In actual physical operation [17,18], either experimental or commercial, the air bubble inflation pressure and modified machine tension are not fixed and are not easy to control tightly. This paper fixes two parameters that are controllable—the bubble air mass, which remains approximately constant once the air inlet valve is shut, and the take-up ratio, which is controlled by the speed of the nip rollers. A dynamic thin-shell model with non-isothermal crystallization kinetic rate and quasi-Newtonian constitutive is simulated using material properties typical of LDPE and laboratory operating conditions (Henrichsen [3] performed steady-state calculations for this model using a microstructural constitutive relation, but these computations were restricted to the quasi-cylindrical model, which gives poor quantitative results when used over a wide range of operating conditions [19]). Regions of stable operations are mapped and under certain conditions, spontaneously oscillating solutions and multiple steady states are generated. A local stability analysis based on the linearized system is conducted to confirm the stability of the operations that appear stable by dynamic simulation. To accomplish this, a double-precision generalized eigenvalue solver DGGEV, from LAPACK [20], was used.

2. Theoretical model for thin film extrusion

Pearson and Petrie and others have developed steady-state models to describe blown film extrusion in the limit of very thin films [21–24]. In these models, variations of the physical variables across the thin film are neglected, leaving the variables as functions of axial position (height above the die) only. Generally, these models involve the continuity equations, momentum equations in the

Please cite this article in press as: J.C. Pirkle Jr., R.D. Braatz, Instabilities and multiplicities in non-isothermal blown film extrusion including the effects of crystallization, J. Process Control (2011), doi:10.1016/j.jprocont.2010.12.007

Table 1
Symbols for dimensional variables and constants.

b	Exponent for the denominator term of the viscosity factor
C_{pf}	Specific heat of polymer (kJ/kg K)
D_{crys}	Width of Gaussian temperature-dependence crystallization function
F_Z	Machine tension (N)
H_0	Film thickness as it exits the die at $Z=0$ (m)
H	Film thickness at axial position Z (m)
H_L	Film thickness at top boundary of freeze zone (m)
k_{crys}	Crystallization rate coefficient (1/s)
L	Axial position corresponding to top of freeze zone (m)
M_{air}	Bubble air mass (mol)
N_Z	Number of grid points in the discretization of the axial coordinate
P_{atm}	Atmospheric pressure
R	Radius of film bubble tube at axial position Z (cm)
R_L	Final radius of film bubble tube at top boundary of freeze zone (m)
R_0	Radius of film bubble tube as it exits the die at $Z=0$ (m)
t	Time (s)
T	Temperature of film bubble tube at position Z (K)
T_{air}	Temperature of cooling air (K)
T_{max}	Temperature at maximum rate of Gaussian crystallization (K)
T_0	Temperature of film bubble tube as it exits die at $Z=0$ (K)
T_{ref}	Reference temperature for normalization of temperature (K)
U_h	Heat transfer coefficient (W/m^2 K)
X	Local fraction of crystallinity (kg crystalline phase/kg polymer)
X_f	Final crystallinity (kg crystalline phase, kg polymer)
V	Velocity of film at axial position Z (m/s)
V_L	Velocity of film at top boundary of freeze zone (m/s)
V_0	Velocity of film as it exits the die at $Z=0$ (m/s)
Z	Axial position measured upward from position of die (m)
α_1	Adjustment coefficient for viscosity factor (Pa s)
α_2	Adjustment coefficient for crystallization term in viscosity factor
β_1	Adjustment coefficient for temperature dependence of viscosity factor (K)
β_2	Exponent for crystallization dependence of viscosity factor
ΔH_{crys}	Heat of crystallization (kJ/kg mole)
ΔP	Inflation pressure, relative to ambient pressure (Pa)
ρ	Polymer density (kg/m^3)
$\Re$	Universal gas constant
μ	Viscosity of polymer (Pa s)
μ_0	Viscosity of polymer as it exits die (Pa s)

Table 2
Symbols for dimensionless variables and constants.

B_1	Inflation pressure force in the microstructural model $= B_1 = \frac{R_0^2 \Delta P}{2H_0 V_0 \mu_0}$
B_2	Heat transfer coefficient $= U_h R_0/\rho C_{pf} H_0 V_0$
B_3	Heat of crystallization $= \Delta H_{crys} X_f / C_{pf} T_{ref}$
B_4	Kinetic coefficient of crystallization $= R_0 k_{crys}/V_0$
B_7	Activation coefficient for viscosity $= \beta_1/T_{ref}$
BUR	Blow-up ratio
F	Modified machine tension
h	Film thickness $= H/H_0$
r	Film bubble-tube radius $= R/R_0$
r_L	Film bubble-tube radius at the top boundary of freeze zone
TUR	Take-up ratio
T_Z	Elongational or machine tension $= \frac{F_Z}{2H_0 V_0 \mu_0}$
x	Crystallinity $= X/X_f$
v	Film velocity $= V/V_0$
v_L	Take-up ratio $= V_L/V_0$
y	Derivative of radius with respect to axial position $= \partial r/\partial \varsigma$
χ	Crystallinity $= X/X_f$
ς	Axial position $= Z/R_0$
η	Viscosity factor $= \mu/\mu_0$
θ	Temperature $= T/T_{ref}$
θ_{air}	Temperature of air $= T_{air}/T_{ref}$
τ	Time $= tV_0/R_0$
ψ	Curvature function

axial and circumferential directions, and some type of constitutive relation. In later applications, these were coupled with equations for energy and crystallization kinetics in order to follow the effect of temperature and crystallization on the viscosity [25,26].

The dynamic model of film motion neglects inertial terms, surface tension, drag effects of the cooling air, and gravity. Dimensionless variables are used in the equations that follow (the dimensional and dimensionless variables are defined in Tables 1 and 2). The axial position variable Z is bounded by $Z=0$ at the die and $Z=L$ at the upper boundary of the Z domain, which is located just below the guide rolls (see Fig. 1). The freeze zone begins at the onset of crystallization and ends where further changes in bubble-tube dimensions are imperceptible due the extremely large viscosity.

In the Pearson–Petrie thin shell model, the dynamic continuity equation takes the dimensionless form [9]:

$$\psi\left(h\frac{\partial r}{\partial \tau}+r\frac{\partial h}{\partial \tau}\right)+\frac{rhy}{\psi}\frac{\partial(\partial r/\partial \varsigma)}{\partial \tau}+rh\frac{\partial v}{\partial \varsigma}+rv\frac{\partial h}{\partial \varsigma}+hv\frac{\partial r}{\partial \varsigma}=0, \quad (1)$$

where $\psi = \sqrt{1+(\partial r/\partial \varsigma)^2}$. The dynamic momentum equation in the axial direction is

$$-\frac{r}{\psi}\frac{\partial h}{\partial \tau}+\frac{rh}{\psi^3}\frac{\partial r}{\partial \varsigma}\frac{\partial\left(\partial r/\partial \varsigma\right)}{\partial \tau}+\frac{rh}{\psi^2}\frac{\partial v}{\partial \varsigma}-\frac{rv}{\psi^2}\frac{\partial h}{\partial \varsigma}=\frac{T_Z+B_1(r^2-r_L^2)}{2\eta}. \quad (2)$$

T_Z is the dimensionless machine tension, B_1 is the dimensionless inflation pressure, and r_L is the value of r at the height $\zeta = L/R_0$ and time τ. The dynamic momentum equation in the circumferential direction is

$$\psi\frac{h}{r^2}\frac{\partial r}{\partial \tau}+\left(\frac{1}{\psi}\frac{\partial^2 r}{\partial \varsigma^2}-\frac{\psi}{r}\right)\frac{\partial h}{\partial \tau}-\frac{h}{\psi^3}\frac{\partial r}{\partial \varsigma}\frac{\partial^2 r}{\partial \varsigma^2}\frac{\partial\left(\partial r/\partial \varsigma\right)}{\partial \tau}$$
$$-\frac{1}{\psi^2}\frac{\partial^2 r}{\partial \varsigma^2}\left(h\frac{\partial v}{\partial \varsigma}-v\frac{\partial h}{\partial \varsigma}\right)+\frac{v}{r^2}\left(h\frac{\partial r}{\partial \varsigma}-r\frac{\partial h}{\partial \varsigma}\right)=\frac{B_1}{\eta}\psi^2. \quad (3)$$

2.1. Energy and crystallization

The energy balance and crystallization equations are

$$\psi\frac{\partial \theta}{\partial \tau}+v\frac{\partial \theta}{\partial \varsigma}+\psi B_2\frac{\theta-\theta_{air}}{h}-B_3B_4F_\theta(1-x)=0, \quad (4)$$

$$\frac{\partial x}{\partial \tau}+\frac{v}{\psi}\frac{\partial x}{\partial \varsigma}-B_4F_\theta(1-x)=0, \quad (5)$$

where

$$B_2=\frac{U_hR_0}{\rho C_{pf}H_0V_0}, \quad (6)$$

$$B_3=\frac{\Delta H_{crys}X_f}{C_{pf}T_{ref}}, \quad (7)$$

$$B_4=\frac{R_0k_{crys}}{V_0}. \quad (8)$$

Heat loss due to radiation is about 20% of that due to convection, so it was lumped into the convective heat-loss term by using a slightly higher heat transfer coefficient. The dimensionless air and wall temperatures are defined as

$$\theta_{air}=\frac{T_{air}}{T_{ref}}, \quad (9)$$

$$\theta_{wall}=\frac{T_{wall}}{T_{ref}}. \quad (10)$$

The function

$$F_\theta=\exp\left[-\frac{4\ln(2)\left(\theta-\theta_{max}\right)^2}{\left(\Delta\theta_{max}\right)^2}\right] \quad (11)$$

Please cite this article in press as: J.C. Pirkle Jr., R.D. Braatz, Instabilities and multiplicities in non-isothermal blown film extrusion including the effects of crystallization, J. Process Control (2011), doi:10.1016/j.jprocont.2010.12.007

is the Gaussian temperature-dependent factor for the rate of crystallization, where the dimensionless constants θ_{max} and $\Delta\theta_{max}$ are

$$\theta_{max} = \frac{T_{max}}{T_{ref}}, \tag{12}$$

$$\Delta\theta_{max} = \frac{D_{crys}}{T_{ref}}. \tag{13}$$

Unlike the Hoffman–Lauritzen kinetic expression, which has five parameters, this expression has three parameters and allows a finite crystallization rate at the die, rather than restricting crystallization to temperatures below the melting point. Like most past studies of blown-film extrusion, with the exception of recent work [2,4–7], flow-induced crystallization is ignored. Extensive calculations performed in examining the effect of flow-induced crystallization indicated that flow-induced crystallization had a moderate effect on results when bubble air mass and take-up speed are held constant [7].

2.2. Boundary and initial conditions

Assuming that a uniform bubble tube of constant radius, film thickness, temperature, film speed, temperature, and zero crystallinity [7,16,19] is attached to the nip rolls at time zero, the initial conditions are

$$r = 1 \quad \text{for} \quad 0 \le \varsigma \le \frac{L}{R_0} \quad \text{at} \quad \tau = 0, \tag{14}$$

$$h = 1 \quad \text{for} \quad 0 \le \varsigma \le \frac{L}{R_0} \quad \text{at} \quad \tau = 0, \tag{15}$$

$$v = 1 \quad \text{for} \quad 0 \le \varsigma \le \frac{L}{R_0} \quad \text{at} \quad \tau = 0, \tag{16}$$

$$\theta = 1 \quad \text{for} \quad 0 \le \varsigma \le \frac{L}{R_0} \quad \text{at} \quad \tau = 0, \tag{17}$$

$$\chi = 0 \quad \text{for} \quad 0 \le \varsigma \le \frac{L}{R_0} \quad \text{at} \quad \tau = 0. \tag{18}$$

The boundary conditions at the die, which are well established in the literature [2–23] are

$$r = 1 \quad \text{at} \quad \varsigma = 0, \tag{19}$$

$$h = 1 \quad \text{at} \quad \varsigma = 0, \tag{20}$$

$$v = 1 \quad \text{at} \quad \varsigma = 0. \tag{21}$$

The corresponding "minimally reduced" outflow boundary condition is

$$\psi \frac{h}{r^2}\frac{\partial r}{\partial \tau} - \left(\frac{\psi}{r}\right)\frac{\partial h}{\partial \tau} + \frac{v}{r^2}\left(h\frac{\partial r}{\partial \varsigma} - r\frac{\partial h}{\partial \varsigma}\right) = \frac{B_1}{\eta}\psi^2 \quad \text{at} \quad \varsigma = \frac{L}{R_0}, \tag{22}$$

which is Eq. (3) with all terms involving $\partial^2 r/\partial\varsigma^2$ removed. The need to use the minimally reduced outflow condition in blown film extrusion is discussed in earlier publications [7,16]. The validity of this type of boundary condition in other applications has also been investigated [27,28]. The value of the top of the simulation domain L (L/R_0 in dimensionless form) was set as the height just below the guide rolls so that the freeze zone and frost line heights are allowed to be established naturally and the results are not a function of the outflow boundary condition. This approach is applicable to this model due to the significant increase in viscosity caused by temperature drop and crystallization.

The temperature and degree of crystallization are specified at the die as

$$\theta = 1 \quad \text{at} \quad \zeta = 0, \tag{23}$$

$$\chi = 0 \quad \text{at} \quad \zeta = 0. \tag{24}$$

2.3. Constraint equations

The solutions to the DAE system are to be generated with prescribed bubble air mass M_{air} and the take-up speed v_L. In the case of no leakage, M_{air} is constant at the value $M_{air,ss}$ after the bubble tube is inflated and the inlet air valve is shut due to the sealing of the bubble by the nip rolls:

$$M_{air,ss} = \frac{P_{atm} + \Delta P}{R_G T_{air}} R_0^3 \pi \int_0^{R_0/L} r^2 d\varsigma \quad \text{for} \quad \tau \to \infty \tag{25}$$

and the take-up speed is set by the speed of the nip rolls:

$$\text{TUR} = v_L \quad \text{for} \; \tau > 0. \tag{26}$$

To model the experimental procedure, TUR was gradually increased from a starting value $v_{L,0}$ to the steady-state value $v_{L,ss}$ by using a switching function:

$$v_L = (v_{L,ss} - v_{L,0})\left(1 - \exp\left(\frac{-\tau^2}{\tau_s^2}\right)\right) + v_{L,0}. \tag{27}$$

As the bubble air mass M_{air} is increased from its initial value by opening the inflation air valve during startup, a differential equation can be formulated as

$$\frac{dM_{air}}{dt} = f_{air,in}, \tag{28}$$

where $f_{air,in}$ is the air flow rate through the inflation valve. The initial condition is

$$M_{air} = M_{air,0} \quad \text{at} \; \tau = 0 \tag{29}$$

In Eq. (28), the inflation air flow rate $f_{air,in}$ can be a time-dependent function that vanishes when M_{air} reaches the desired quantity $M_{air,ss}$. In the calculations reported here, the inflation air flow rate takes the form

$$f_{air,in} = (M_{air} - M_{air,0})\left(\frac{2\tau}{\tau_s^2}\right)\exp\left(\frac{-\tau^2}{\tau_s^2}\right). \tag{30}$$

In case of an air leak at the nip rolls, the inflation airflow rate can be used to compensate for the leak. Such a flow rate can be determined by a control strategy that that monitors inflation pressure and bubble size and shape, which are measurable using a pressure transducer, a CCD camera, and imaging software (e.g., as described in [48]).

With the additional constraint Eqs. (27) and (28), two new dependent variables need to be added for the system to be well-posed. These are the modified machine tension F, where $F = T_Z - Br_L^2$, and the dimensionless inflation pressure B_1. The variables F and B_1 depend only upon time, so the equations

$$\frac{\partial F}{\partial \varsigma} = 0 \tag{31}$$

and

$$\frac{\partial B_1}{\partial \varsigma} = 0 \tag{32}$$

hold. For consistency, the initial conditions for F and B_1 are set to

$$F = 0 \quad \text{at} \quad \tau = 0, \tag{33}$$

$$B_1 = 0 \quad \text{at} \; \tau = 0. \tag{34}$$

2.4. Constitutive relation

A non-isothermal Newtonian constitutive relation was used for LLDPE that allows for the effect of temperature and crystallization on the viscosity of the extruded polymer. Mathematically, the viscosity is given by

$$\mu = \mu_0 \eta, \tag{35}$$

Please cite this article in press as: J.C. Pirkle Jr., R.D. Braatz, Instabilities and multiplicities in non-isothermal blown film extrusion including the effects of crystallization, J. Process Control (2011), doi:10.1016/j.jprocont.2010.12.007

where the base viscosity μ_0 is

$$\mu_0 = \alpha_1 \exp\left(\frac{\beta_1}{T_0}\right) \tag{36}$$

and the dimensionless viscosity factor η, which accounts for temperature change and crystallization, is

$$\eta = \exp\left[\frac{\beta_1}{T_0}\left(\frac{1}{\theta} - 1\right)\right] \exp(\alpha_2 \chi^{\beta_2}), \tag{37}$$

where α_1, α_2, β_1, β_2, and b are measured or adjusted constants.

2.5. Heat transfer function

The coefficient of heat transfer U_h from the film to the external air is a function of position Z above the die. The air from the air ring is assumed to impinge on the bubble surface at $\zeta \sim 1.6$. Turbulent flow simulations [29] show that the heat transfer coefficient reaches a maximum before dropping to a lower value, which is described by

$$B_2 = B_{2,0} F_u. \tag{38}$$

Here

$$F_u = \begin{cases} 0, & 0 \le \varsigma < A_H \\ 2\,(\varsigma - A_H) \exp\left(-\dfrac{\varsigma - A_H}{B_H}\right), & A_H \le \varsigma < C_H \\ D_H, & C_H \le \varsigma < L/R_0 \end{cases} \tag{39}$$

where $\varsigma = Z/R_0$. The magnitude of U_{h0} is generally larger for larger external air flow around the bubble.

2.6. Well-posedness of PDAE system

To facilitate analysis of the nonlinear PDAE system for well-posedness, it is best to reformulate Eqs. (1)–(3) by defining a dependent variable $y \equiv \partial r/\partial \varsigma$. Eqs. (1)–(3) then take the form

$$\psi\left(h\frac{\partial r}{\partial \tau} + r\frac{\partial h}{\partial \tau}\right) + \frac{rhy}{\psi}\frac{\partial y}{\partial \tau} + rh\frac{\partial v}{\partial \varsigma} + rv\frac{\partial h}{\partial \varsigma} + hvy = 0, \tag{40}$$

$$-\frac{r}{\psi}\frac{\partial h}{\partial \tau} + \frac{rhy}{\psi^3}\frac{\partial y}{\partial \tau} + \frac{rh}{\psi^2}\frac{\partial v}{\partial \varsigma} - \frac{rv}{\psi^2}\frac{\partial h}{\partial \varsigma} = \frac{F + B_1 r^2}{2\eta}, \tag{41}$$

$$\psi\frac{h}{r^2}\frac{\partial r}{\partial \tau} + \left(\frac{1}{\psi}\frac{\partial y}{\partial \varsigma} - \frac{\psi}{r}\right)\frac{\partial h}{\partial \tau} - \frac{hy}{\psi^3}\frac{\partial y}{\partial \varsigma}\frac{\partial y}{\partial \tau} - \frac{1}{\psi^2}\frac{\partial y}{\partial \varsigma}\left(h\frac{\partial v}{\partial \varsigma} - v\frac{\partial h}{\partial \varsigma}\right) + \frac{v}{r^2}\left(hy - r\frac{\partial h}{\partial \varsigma}\right) = \frac{B_1}{\eta}\psi^2. \tag{42}$$

where $\psi \equiv \sqrt{1 + y^2}$ and the modified tension variable F has been substituted for $F \equiv T_Z - B_1 r_L^2$. As the radius of the bubble tube is constant at time zero, the initial condition for y is

$$y = 0 \quad \text{for} \quad 0 \le \varsigma \le \frac{L}{R_0} \quad \text{at} \quad \tau = 0. \tag{43}$$

For these governing equations, the set of dependent variables is $\{r, h, v, y, \theta, \chi, F, B_1\}$, and the control variables are $M_{\text{air,ss}}$ and $TUR \equiv v_L$. Application of the methods for analysis of a PDAE system [30] indicates that there are eight degrees of freedom with respect to the independent variable τ. This corresponds to the number of initial conditions: Eqs. (14)–(18), (33), (34), and (43). The same procedure determines that there are seven degrees of freedom with respect to the independent variable ς, corresponding to the number of boundary conditions: Eqs. (19)–(24) and (27). From this analysis, the PDAE system appears to be well posed.

3. Numerical calculations

3.1. Solution of system of equations

The above system of algebraic and partial differential equations can be solved using the numerical method of lines (NMOL) [31]. This involves discretizing the equations in the spatial variable ς at a number of grid points N_Z. Spatial derivatives such as $\partial v/\partial \varsigma$ were approximated as five-point finite differences in order to achieve 4th-order accuracy with the spatial variable eliminated as an independent variable. A variable-grid spacing technique that allowed a choice of such 5-point finite differences for first derivatives was coded in the subroutine DSS032 [32]. The formula of Fornberg [33] was used for the second-order derivative $\partial^2 r/\partial \varsigma^2$. The spatial discretization converts the system equations, including boundary conditions, to a set of ordinary differential-algebraic equations that were solved using the double-precision version of the solver DASPK3.0 [34,35]. All computations were performed in double-precision Fortran 90 using a 2.66 GHz Intel quad-core processor-based computer with 8 GB of DRAM. Other discretization schemes were tried, such as 3-point finite differences and 4th-order orthogonal collocation on finite elements. The 5-point finite difference approximation gave the highest accuracy for the same number of grid points. This is in agreement with the findings of other investigators [36].

Once subjected to spatial discretization, Eqs. (1)–(39) form a DAE system with respect to the independent variable τ (dimensionless time). Application of index analysis methods from the literature [37–39] indicated that the differential index of the DAE system is one, which the chosen DAE solver, DASPK3.0, readily handles [32].

To assess the number of grid points required for accuracy, N_z was varied from 51 to 1001. Using a least-squares error function based upon all normalized dependent variables, $N_z = 251$ was found to produce simulation results within 0.0001% of those obtained for $N_z = 1001$. More grid points were placed between the die and the end of the frost zone because the changes in bubble geometry occurred in this region. Beyond the frost zone, the bubble dimensions were relatively flat. All results reported in this paper used 251 grid points with 70% of the points placed in the first 40% of the axial domain.

3.2. Stability analysis

Local asymptotically stability about a steady-state is implied if all of the generalized eigenvalues of the linearized system of equations:

$$\mathbf{\Omega} = \tag{44}$$

have negative real part [40], where $\mathbf{x}$ is the vector of perturbations, and $\mathbf{M}$ is a matrix that can be singular, and the matrix $\mathbf{A}$ can be asymmetric. Both $\mathbf{A}$ and $\mathbf{M}$ are large and sparse. Software is available for computing generalized eigenvalues for singular $\mathbf{M}$ and asymmetric $\mathbf{A}$ (see [41–43] and citations therein). For a test range of grid points, the LAPACK full-matrix routine DGGEV [20] was used as the generalized eigenvalue solver. Too few grid points can yield incorrect generalized eigenvalues, which would result in an unreliable location of stability zones (see [45] for more detailed discussion). The results of DGGEV were occasionally double-checked using a second generalized eigenvalue solver, ARPACK [44].

3.3. Model input conditions

The model parameter values are listed in Table 3. The material properties of the LLDPE polymer were obtained from a compendium of data in the literature on LLDPE [4,23,46]. For the viscosity parameters, correlations and data from the three papers

Please cite this article in press as: J.C. Pirkle Jr., R.D. Braatz, Instabilities and multiplicities in non-isothermal blown film extrusion including the effects of crystallization, J. Process Control (2011), doi:10.1016/j.jprocont.2010.12.007

Table 3
Values of parameters used in the simulations.

A_H	1.6
b	0.68
B_H	1.5
C_H	4.6
C_{pf}	2.51 kJ/kg K
D_H	0.3
H_0	0.05 cm
k_{crys}	0.37 s^{-1}
R_0	1.25 cm
T_{air}	319 K
T_{max}	368 K
ΔT_{max}	5 K
T_0	481.2 K
TUR	1.10–4.40
U_{h0}	48.18–52.36 W/m^2 K
V_0	0.46803 cm/s
X_f	0.562
α_1	1.828 Pa s
α_2	13.5
β_1	3969.4 K
β_2	0.4
λ_a	0.0 s
ΔH_{crys}	251 kJ/kg
ΔP	40.36–65.47 Pa
ρ	922 kg/m^3
τ_s	100.0

were averaged into one correlation. The dimensions of the extrusion apparatus correspond to a laboratory experimental unit at the University of Illinois [48].

4. Results and discussion

4.1. Steady-state correlations of dependent variables

This section provides plots of the stable steady-states identified by the linearized system as having all generalized eigenvalue(s) with negative real part as reported in Table 4 (dynamic instabilities are considered in the Section 4.2). To simplify the notation, the generalized eigenvalues with the highest real part are referred to as dominant eigenvalues.

4.1.1. Effect of bubble air mass

Having a fixed bubble air mass constrains the blow-up ratio for stable steady-state operation within a narrow range, while the corresponding thickness reduction varies widely (see Fig. 2a). The stable steady-state value for the thickness reduction is observed to increase approximately linearly with the take-up ratio, with this relationship being a relatively weak function of bubble air mass (see Fig. 2b). The highest value for the thickness reduction of 16.5 observed for stable operations in Fig. 2b corresponds to the middle value for the bubble air mass M_{air} = 0.1266 mol, indicating that an optimal intermediate value for the bubble air mass M_{air} exists if the operational objective is to maximize thickness reduction. The ranges of the take-up ratio and thickness reduction for stable operation are larger for M_{air} = 0.1266 mol than for M_{air} = 0.1097 and 0.1435 mol.

Increasing the take-up ratio at constant bubble air mass M_{air} corresponds to a higher effective bubble pressure B_1 (see Fig. 2c). The intersection of the curves in Fig. 2c indicates that the same stable values for the take-up ratio and inflation pressure force B_1 can be achieved by different values for the bubble air mass. The blow-up ratio for stable operations is observed to increase with inflation pressure force B_1 (see Fig. 2d). Stable values for the bubble air mass and take-up ratio correspond to a relatively large range of inflation pressures.

4.1.2. Effect of cooling air rate

Modest increases in the cooling air rate correspond to modest increases in the convective heat transfer, which results in take-up ratio and thickness reduction curves that nearly lie on top of each other (see Fig. 3a). The range of take-up ratio for stable operation, however, is different, with the highest cooling rate corresponding to the greater possible thickness reduction. The blow-up ratio declines somewhat with increased cooling ratio (see Fig. 3b), which is commercially less important than the potential increase in thickness reduction (Fig. 3a). The required bubble inflation pressure force B_1 increases with cooling rate (see Fig. 3c). This is not surprising, as the increased viscosity at lower temperatures offers greater resistance to inflation. A monotonic dependence of blow-up ratio upon the inflation pressure force B_1 no longer holds at the higher cooling rate (see curve for U_{h0} = 52.36 W/m^2 K in Fig. 3d). This nonconformance occurs only at the lower values of blow-up ratio and thickness reduction, which is unlikely to correspond to a desired

Table 4
Steady-state results for bubble air mass M_{air} = 0.1013 mol, Heat transfer coefficient U_{h0} = 48.18 W/m^2 K, and other parameters in Table 3.

TUR	Inflation pressure force B_1	Machine tension T_Z	Thickness reduction	Blow-up ratio	Re{λ_{max}}[a]	Im{λ_{max}}[a]	Oscillations
1.2000	0.19581	3.03723	4.65899	3.88249	−0.0159	0.7288	No
1.3000	0.20147	3.18494	5.06198	3.89383	−0.0260	0.7724	No
1.4000	0.20675	3.32227	5.46603	3.90432	−0.0297	0.3011	No
1.6000	0.21639	3.57139	6.27706	3.92317	−0.0286	0.7411	No
1.8000	0.22502	3.79309	7.09156	3.93976	−0.0262	0.8257	No
2.0000	0.23283	3.99298	7.90897	3.95450	−0.0281	0.9037	No
2.2000	0.23997	4.17525	8.72914	3.96780	−0.0345	0.9764	No
2.4000	0.24655	4.34289	9.55168	3.97988	−0.0450	1.0437	No
2.6000	0.25266	4.49818	10.37642	3.99095	−0.0417	0.5995	No
2.8000	0.25836	4.64292	11.20318	4.00115	−0.0344	0.6472	No
3.0000	0.26371	4.77851	12.03179	4.01061	−0.0236	0.6910	No
3.2000	0.26874	4.90612	12.86213	4.01943	−0.0101	0.7292	No
3.3000	0.27115	4.96721	13.27798	4.02363	−0.0039	0.7457	No
3.3500	0.27233	4.99712	13.48595	4.02567	−0.0010	0.7546	No
3.3636	0.27265	5.00519	13.54256	4.02622	0.0002	0.7563	Yes (small)
3.4000	0.27349	5.02665	13.69414	4.02769	0.0026	0.7626	Yes (small)
3.5000	0.27578	5.08452	14.11067	4.03163	0.0082	0.7776	Yes (small)
3.6000	0.27801	5.14085	14.52779	4.03540	0.0130	0.7928	Yes (small)
3.7000	0.28017	5.19595	14.94454	4.03916	0.0179	0.8076	Yes
3.8000	0.28224	5.24900	15.36093	4.04284	0.0221	0.8187	Yes

[a] Real and imaginary parts for the generalized eigenvalues of (42) that have the largest real part.

Please cite this article in press as: J.C. Pirkle Jr., R.D. Braatz, Instabilities and multiplicities in non-isothermal blown film extrusion including the effects of crystallization, J. Process Control (2011), doi:10.1016/j.jprocont.2010.12.007

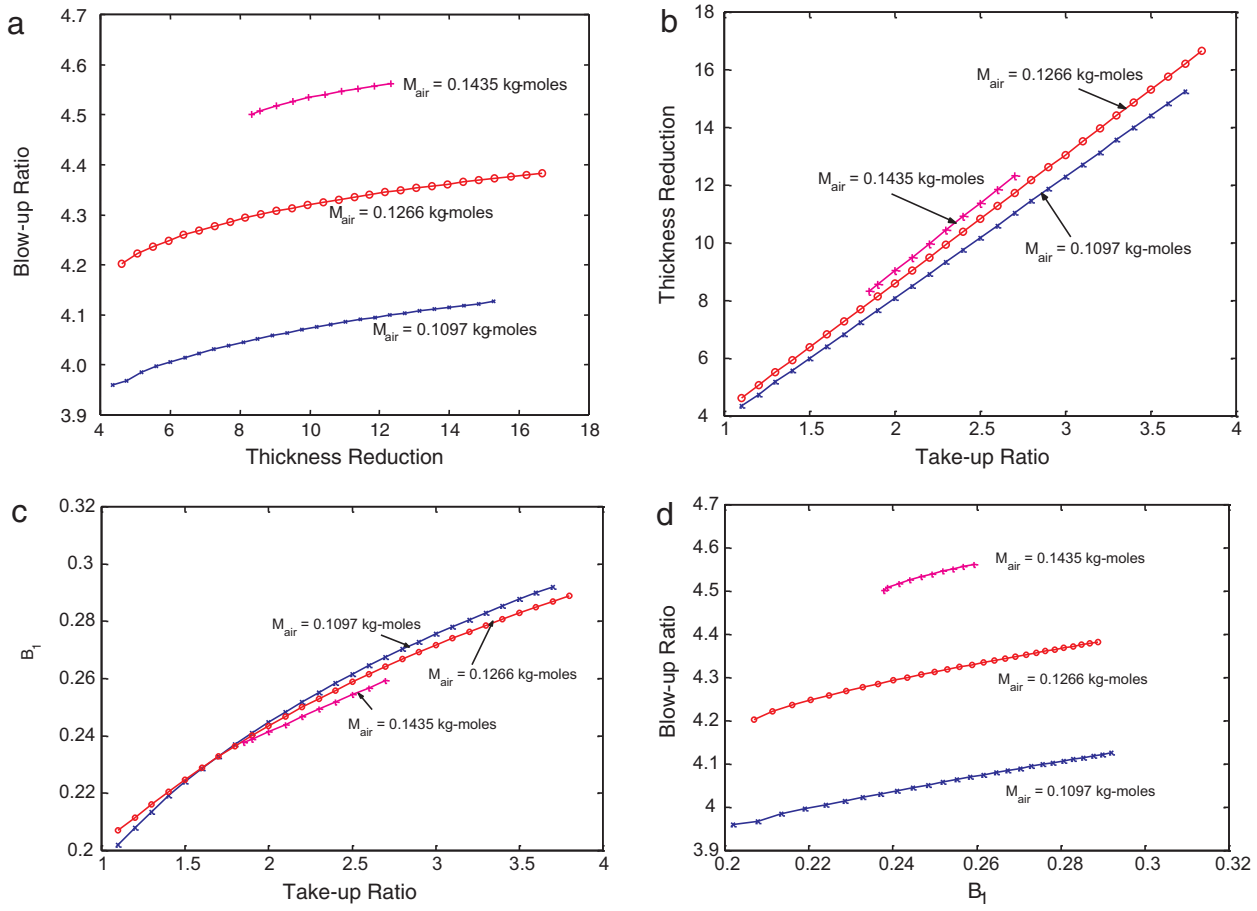

Fig. 2. (a) Blow-up ratio versus thickness reduction, (b) thickness reduction versus take-up ratio, (c) inflation pressure force B_1 vs. take-up ratio, and (d) blow-up ratio versus inflation pressure force B_1 for three values of bubble air mass M_{air}, $U_{h0} = 50.27\ \mathrm{W/m^2\ K}$, and other parameters in Table 3.

operating condition. Most of these observations are well known and have been discussed by Cantor [39], among others.

4.2. Dynamic instabilities

4.2.1. Oscillations

Several papers have investigated draw resonance and helical instabilities in film blowing [12–14], which occur at high and low take-up ratios, respectively. The models in those papers included non-isothermal processing and the Phan–Thien Tanner rheological relation but did not include crystallization. Here these instability phenomena are explored for the Newtonian non-isothermal thin-shell model with crystallization, by use of dynamic simulation.

Key steady-state operating parameters for low bubble air mass and cooling air flowrate with the dominant eigenvalues from linearized analysis are reported in Table 4 for a fixed bubble air mass and heat transfer coefficient and range of take-up ratio, with the last column indicating whether the dynamic simulations near those steady-states are observed to be oscillatory. The dominant eigenvalues indicate that the steady-state solutions for a take-up ratio from 1.2 to 3.35 are locally asymptotically stable.

Oscillations in the thickness reduction and machine tension are observed for a take-up ratio of 1.1 or less. These oscillations have been observed to be associated with a helical instability [13,14,18,47]. Precise quantification of the process states during a helical instability requires a three-dimensional model of bubble geometry rather than the thin-shell model which assumes axial symmetry. Commercial operation of blown film extruders is concerned with operations at higher take-up ratio, which corresponds to greater thickness reduction of the film. Stable operation is also bounded for higher take-up ratios. For a take-up ratio larger than 3.35, another type of instability arises that is called the draw-resonance instability in agreement with Refs. [13–15] (while other researchers [40] refer to the instability for high take-up ratio as "bubble instability" and instability for blow-up ratio less than 1 as "draw-resonance instability," this paper uses the nomenclature in Refs. [13–15] as operations with blow-up ratio less than 1 are not commercially relevant). The onset of this instability is accompanied by larger values in the machine tension T_Z (see Table 4). For a take-up ratio of 3.8, the draw-resonance instability is clearly seen in dynamic simulations (see Fig. 4a and b). The instability that occurs at take-up ratio >3.35 can be modeled by the thin-shell model.

The oscillations in Fig. 4a and b occurred spontaneously during the startup period of the simulations. Initially the values of the thickness reduction, machine tension, blow-up ratio, and inflation pressure approached the values at the unstable steady-state that then transitioned into a sustained oscillation. To assess whether insufficient spatial resolution in the discretization step caused instability and subsequent oscillation, the number of grid points was varied from 50 to 751. The stability maps and the periods of oscillation in Fig. 4a and b were not affected by grid size for $N_Z > 251$.

Please cite this article in press as: J.C. Pirkle Jr., R.D. Braatz, Instabilities and multiplicities in non-isothermal blown film extrusion including the effects of crystallization, J. Process Control (2011), doi:10.1016/j.jprocont.2010.12.007

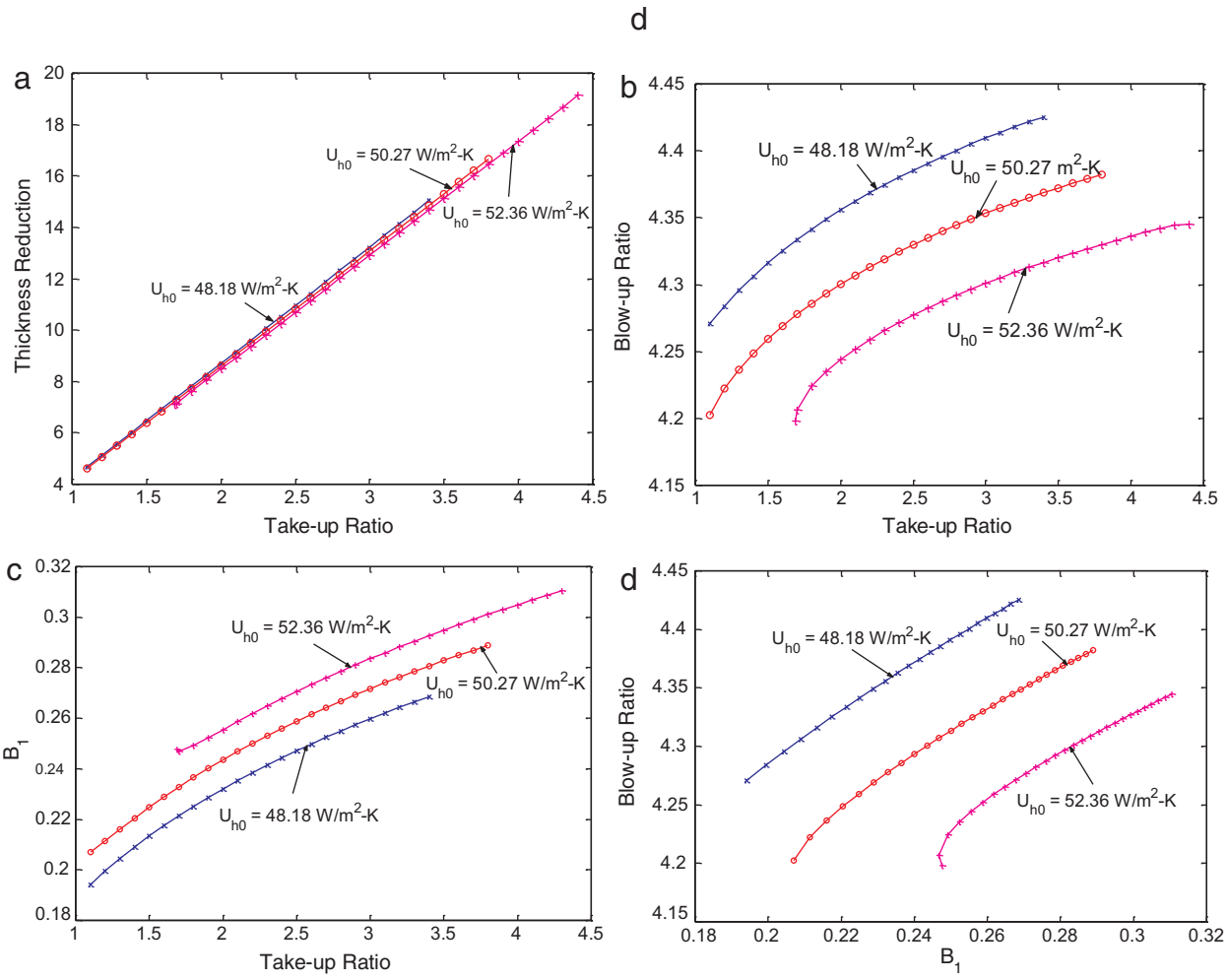

Fig. 3. (a) Thickness reduction versus take-up ratio, (b) blow-up ratio versus take-up ratio, (c) inflation pressure force B_1 vs. take-up ratio, and (d) blow-up ratio versus inflation pressure force B_1 for three values of the heat transfer coefficient U_{h0}, bubble air mass M_{air} = 0.1097 kg-mol, and other parameters in Table 3.

4.2.2. Stability zone

For blown film extrusion, previous investigators have examined multiple steady states, hysteresis, and stability using plots of blow-up ratio versus thickness reduction [8,10–15]. In this paper, these curves were generated in two ways. In the first method, the simulated inflation pressure force B_1 is held constant while the modified machine tension F is varied from a maximum value F_{max} to a minimum value F_{min} [16]. The procedure is then repeated for different constant values of B_1. Fig. 5a and b plot steady-states for the parametric values in Table 3 and U_{h0} = 48.18 W/m^2 K.

The more horizontal upper branches of these curves correspond to lower values of the modified machine tension F, while the lower branches correspond to higher F values. Above F_{max} and below F_{min}, the solutions to the system equations do not converge to a steady-state value. Points on the curves in Fig. 5a correspond to both stable and unstable solutions. Anywhere between zero and three steady-state values for the inflation pressure force can exist for each fixed value for the thickness reduction.

Fig. 5b plots the stable portions of the blow-up ratio versus thickness reduction curves, that is, for steady-state solutions in which the dominant eigenvalues for the linearized system at constant bubble air mass M_{air} and take-up ratio have negative real components. In Fig. 5b, lines of constant take-up ratio are drawn through some of the constant-B_1 blow-up ratio-versus-thickness reduction curves to demonstrate the occurrence of multiple stable steady-states for some values of the inflation pressure force B_1. For an inflation pressure force of B_1 = 0.22, the line with TUR = 1.711 intersects the blowup ratio versus thickness reduction curve three times, indicating the existence of three stable steady states. Likewise, the B_1 = 0.23 curve is intersected three times by the TUR = 2.067 line. The inflation pressure force B_1 = 0.24 and 0.25 curves have two stable steady states for TUR = 2.363 and 2.629, respectively.

A stability zone obtained by the above procedure is mapped in Fig. 6a, which includes an assemblage of stable curves of constant B_1 enveloped by a dotted line. Inside the dotted line, the steady states are stable. The second method used to generate the blow-up ratio-vs.-thickness reduction curves involved holding the simulated bubble air mass constant and varying the take-up ratio. The steady states generated by this procedure were subjected to stability analysis, and Fig. 6b was generated. Here, the assemblage of curves (at different constant values of M_{air}) lying within the dotted envelope represent stable steady states. The comparison between Fig. 6a and b is interesting. There is a region in Fig. 6b (in the upper right-hand corner) that is not present in Fig. 6a. That is, holding the inflation pressure force B_1 constant and varying the modified machine tension F may not readily yield all stable steady-state solutions. This indicates that the preferred method of mapping out the stability region is to prescribe the bubble air mass M_{air} and vary the take-up ratio.

Please cite this article in press as: J.C. Pirkle Jr., R.D. Braatz, Instabilities and multiplicities in non-isothermal blown film extrusion including the effects of crystallization, J. Process Control (2011), doi:10.1016/j.jprocont.2010.12.007

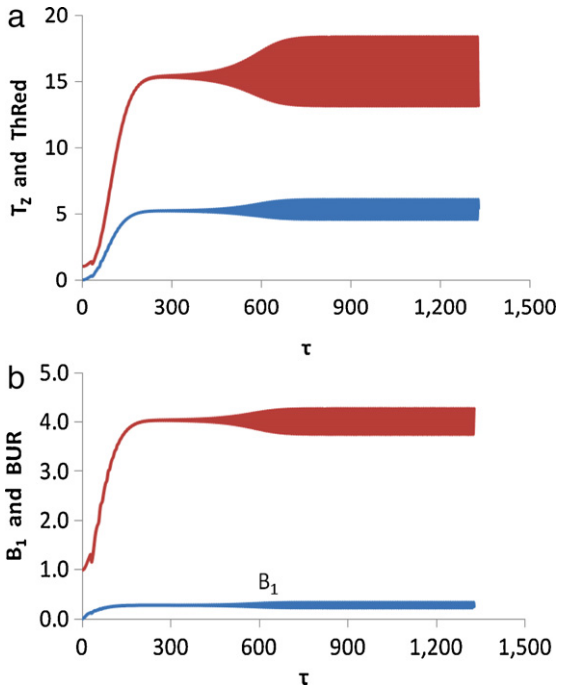

Fig. 4. Oscillations in (a) thickness reduction and machine tension T_Z and (b) blow-up ratio BUR and inflation pressure force B_1 showing draw resonance instability for take-up ratio TUR = 3.8, bubble air mass M_{air} = 0.1013 mol, heat transfer coefficient U_{h0} = 48.18 W/m^2 K, and other parameters in Table 3.

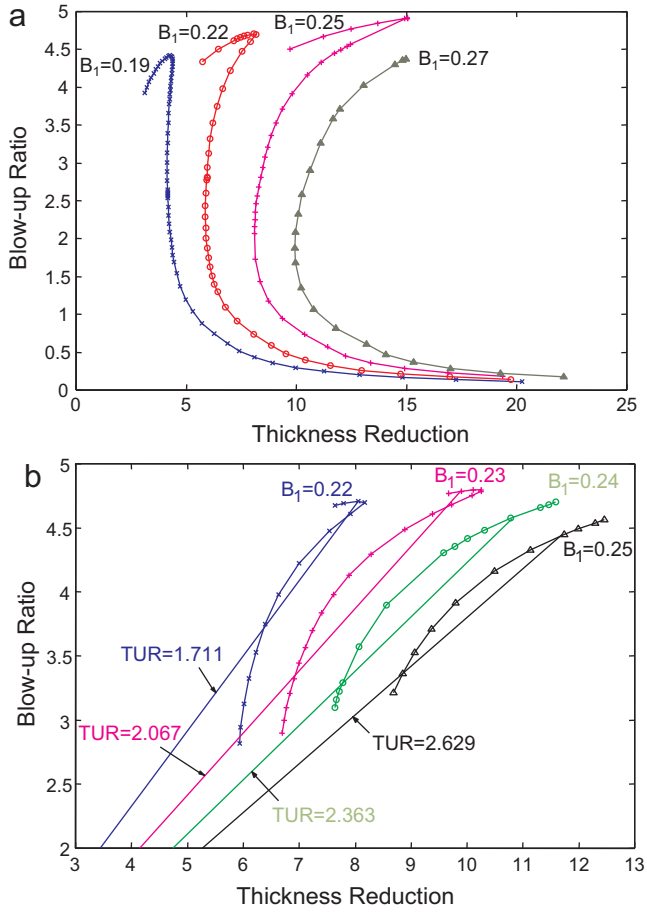

Fig. 5. (a) Typical blow-up ratio versus thickness reduction curves and (b) stable portions of the blow-up ratio versus thickness reduction curves with lines of constant take-up ratio, for constant values of the inflation pressure force B_1, heat transfer coefficient U_{h0} = 48.18 W/m^2 K, and other parameters in Table 3.

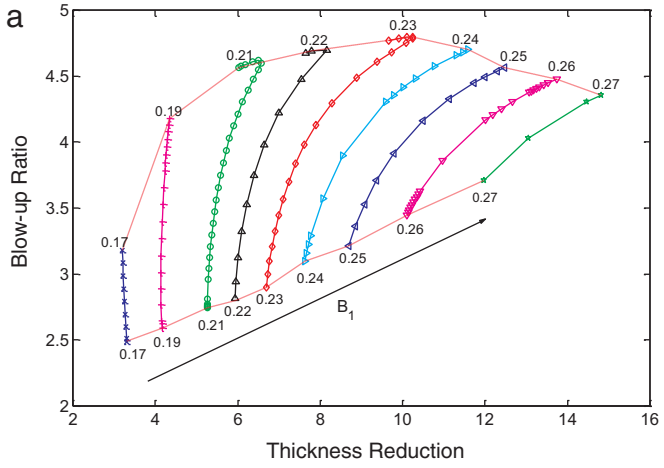

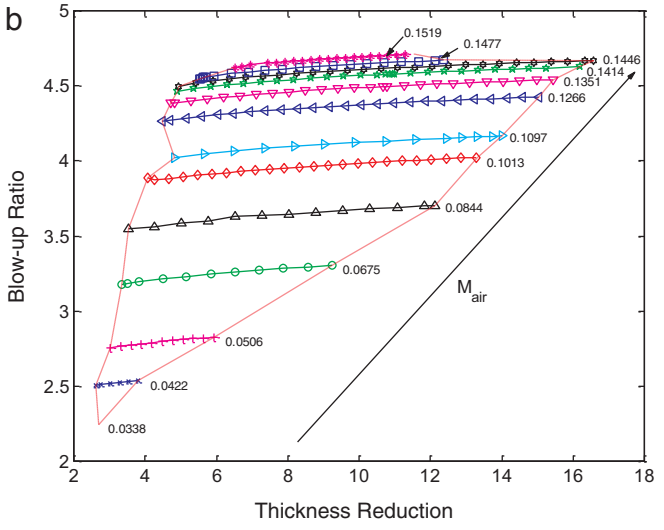

Fig. 6. (a) Stability region of blow-up ratio versus thickness reduction obtained by generating curves of constant inflation pressure force B_1, with the region inside of the dotted line being stable at constant bubble air mass M_{air} and take-up ratio; (b) Stability region of blow-up ratio versus thickness reduction obtained by generating curves of constant bubble air mass M_{air} with the region inside of the dotted line being stable at inflation pressure force B_1 and take-up ratio. The heat transfer coefficient U_{h0} = 48.18 W/m^2 K and other parameters are in Table 3.

5. Conclusions

A straightforward way of generating transient and steady-state solutions to the system of equations governing blown film extrusion is to hold the bubble air mass and take-up ratio constant. The bubble air mass M_{air} and take-up ratio are more controllable than the bubble inflation pressure and machine tension. In addition, the complete zone of stability is generated more readily by holding M_{air} and take-up ratio constant, and then treating the machine tension and bubble inflation pressure as dependent variables. Spontaneous oscillations representing either helical or draw-resonance instabilities are also revealed for conditions lying outside the stability zones.

Curves of either blow-up ratio or thickness reduction-vs.-take-up ratio revealed that there are take-up ratios where zero, one, two, or three steady-state solutions exist. The stability of each stable steady-state solution was analyzed by computing the generalized eigenvalues for the linearized differential-algebraic system. The heat transfer coefficient from the polymer film to the external air and surroundings has a marked influence on the qualitative and quantitative features of the blow-up ratio versus thickness reduction curves. Recommendations were provided on how to most

Please cite this article in press as: J.C. Pirkle Jr., R.D. Braatz, Instabilities and multiplicities in non-isothermal blown film extrusion including the effects of crystallization, J. Process Control (2011), doi:10.1016/j.jprocont.2010.12.007

efficiently and reliably map out the stability region for blown-film extrusion.

Acknowledgement

Support is acknowledged from Procter and Gamble.

References

[1] S. Middleman, Fundamental Studies of Polymer Processing, McGraw-Hill, New York, 1977.
[2] A.K. Doufas, A.J. McHugh, Simulation of film blowing including flow-induced crystallization. Model development and predictions, J. Rheol. 45 (2001) 1085–1104.
[3] L.K. Henrichsen, Modeling of Film Blowing, MS thesis, Department of Chemical Engineering, University of Illinois, Urbana-Champaign, Urbana, IL, USA, 2002.
[4] L.K. Henrichsen, A.J. McHugh, S.S. Cherukupalli, A.A. Ogale, Microstructure and kinematic aspects of blown film extrusion process: II. Numerical modeling and prediction of LLDPE and LDPE, Plastics, Rub. Comp. 33 (2004) 383–389.
[5] L.K. Henrichsen, A.J. McHugh, Analysis of film blowing with flow-enhanced crystallization. Part. I. Steady-state behavior, Intern. Polymer Process. 22 (2007) 179–189.
[6] L.K. Henrichsen, A.J. McHugh, Analysis of film blowing with flow-enhanced crystallization. Part. II. Linearized sensitvity and stability behavior, Intern. Polymer Process. 22 (2007) 190–197.
[7] J.C. Pirkle Jr., R.D. Braatz, A thin-shell two-phase microstructural model for blown film extrusion, J. Rheol. 54 (2010) 471–505.
[8] J.J. Cain, M.M. Denn, Multiplicities and instabilities in film blowing, Polym. Eng. Sci. 28 (1988) 1527–1541.
[9] O. Akaike, T. Tsuiji, Y. Nagano, Simulation of blown-film process taking account of cooling air effect, Intern. Polym. Process. 14 (1999) 168–174.
[10] K.-S. Yoon, C.-W. Park, Stability of a blown film extrusion process, Intern. Polymer Process XIV (1999) 342–349.
[11] Y.L. Yeow, Stability of tubular film flow: A model of the film blowing process, J. Fluid Mech. 75 (1976) 577–591.
[12] K.-S. Yoon, C.-W. Park, Stability of a two-layer blown film extrusion, J. Non-Newtonian Fluid Mech. 89 (2000) 97–116.
[13] J.C. Hyun, H. Kim, J.S. Lee, S. Song, W.W. Jung, Transient solutions of the dynamics in film blowing processes, J. Non-Newtonian Fluid Mech. 121 (2004) 151–162.
[14] J.S. Lee, H.-S. Song, H.W. Jung, J.C. Hyun, Existence of optimal cooling conditions in the film blowing process, J. Non-Newtonian Fluid Mech. 137 (2006) 24–30.
[15] D.M. Shin, J.S. Lee, H.W. Jung, J.C. Hyun, Multiplicity, bifurcation, stability and hysteresis in dynamic solutions of film blowing processes, J. Rheol. 51 (2007) 605–621.
[16] J.C. Pirkle Jr., R.D. Braatz, Dynamic modeling of blown film extrusion, Polym. Eng. Sci. 43 (2003) 398–418.
[17] K. Cantor, Blown Film Extrusion: An Introduction, Hanser, Munich, 2006.
[18] T.I. Butler, Blown film bubble instability induced by fabrication conditions, SPE ANTEC Technical Paper 46 (2000) 156-164.
[19] J.C. Pirkle Jr., R.D. Braatz, Comparison of the dynamic thin shell and quasi-cylindrical models for blown film extrusion, Polym. Eng. Sci. 44 (2004) 1267–1276.
[20] E. Anderson, Z. Bai, C. Bischof, S. Blackford, J. Demmel, J. Dongarra, J. Du Croz, A. Greenbaum, S. Hammarling, A. McKenney, D. Sorensen, LAPACK Users' Guide, Third Ed., SIAM, Philadelphia, 1999.
[21] J.R.A. Pearson, C.J.S. Petrie, The flow of a tubular film. Part 1. Formal mathematical representation, J. Fluid Mech. 40 (1970) 1–19, part 1.
[22] J.R.A. Pearson, C.J.S. Petrie, The flow of a tubular film. Part 2. Interpretation of the model and discussion of the solutions, J. Fluid Mech. 42 (1970) 609–625.
[23] C.J.S. Petrie, A comparison of theoretical predictions with published experimental measurements on the blown film process, AIChE J. 21 (1975) 275–282.
[24] K.-S. Yoon, C.-W. Park, Analysis of isothermal two-layer blown film coextrusion, Polym. Eng. Sci. 32 (1992) 1771–1777.
[25] S.M. Alaie, T.C. Papanastasiou, Modeling of nonisothermal film blowing with integral constitutive equations, Intern. Polym. Process 8 (1993) 51–65.
[26] C.-C. Liu, D.C. Bogue, J.E. Spruiell, Tubular film blowing. Part 2. Theoretical modelling, Intern. Polym. Process. 10 (1995) 230–236.
[27] R.A. Novy, H.T. Davis, L.E. Scriven, A comparison of synthetic boundary conditions, Chem. Eng. Sci. 46 (1991) 57–68.
[28] W.E. Schiesser, PDE boundary conditions from minimum reduction of the PDE, Appl. Numer. Math. 28 (1996) 171–179.
[29] V. Sidiropoulos, P.E. Wood, J. Vlachopoulos, The aerodynamics of cooling of blown film bubbles, J. Reinf. Plast. Compos. 18 (1999) 529–538.
[30] W.S. Martinson, P.I. Barton, A differentiation index for partial differential–algebraic equations, SIAM J. Sci. Comput. 21 (2000) 2295–2315.
[31] W.E. Schiesser, The Numerical Method of Lines Integration of Partial Differential Equations, Academic Press, San Diego, 1991.
[32] C.A. Silebi, W.E. Schiesser, Dynamic Modeling of Transport Process Systems, Academic Press, San Diego, 1992, p. 409.
[33] B. Fornberg, Calculation of weights in finite-difference formulas, SIAM Rev. 40 (1998) 685–691.
[34] T. Maly, L.R. Petzold, Numerical Methods, Software for Sensitivity Analysis of Differential-Algebraic Systems, Appl. Numer. Math. 20 (1996) 57–79.
[35] L.R. Petzold, A description of DASSL: A differential/algebraic system solver, in: R.S. Stepleman (Ed.), Scientific Computing, IMACS, North-Holland, 1983, pp. 65–68.
[36] W.E. Schiesser, G.W. Griffiths, A Compendium of Partial Differential Equation Models: Method of Lines Analysis with Matlab, Cambridge University Press, New York, 2009.
[37] C.C. Pantelides, The consistent initialization of differential-algebraic systems, SIAM J. Sci. Statist. Comput. 9 (1988) 213–231.
[38] J. Unger, A. Kroner, W. Marquardt, Structural analysis of differential-algebraic equation systems - Theory and applications, Comp. Chem. Eng. 19 (1995) 867–882.
[39] K.E. Brenan, S.L. Campbell, L.R. Petzold, Numerical Solution of Initial-Value Problems in Differential-Algebraic Equations, North-Holland, New York, 1989.
[40] T. Stykel, On criteria for asymptotic stability of differential–algebraic equations, Angew. Math. Mech. 82 (2002) 147–158.
[41] J. Demmel, B. Kågström, The generalized Schur decomposition of an arbitrary pencil A–λB: Robust software with error bounds and applications. Part I: theory and algorithms, Acm. T. Math. Software 19 (1993) 160–174.
[42] J. Demmel, B. Kågström, The generalized Schur decomposition of an arbitrary pencil A–λB: Robust software with error bounds and applications. Part II: software and applications, Acm. T. Math. Software 19 (1993) 175–201.
[43] M.A. Freitag, A. Spence, Convergence theory for inexact inverse iteration applied to the generalised nonsymmetric eigenproblem, Electron. Trans. Num. Anal. 28 (2007) 40–64.
[44] R.B. Lehoucq, D.C. Sorensen, C. Yang, ARPACK User's Guide: Solution of Large Scale Eigenvalue Problems with Implicitly Restarted Arnoldi Methods, October 8 (1997).
[45] Y. Liu, E.W. Jacobsen, On the use of reduced order models in bifurcation analysis of distributed parameter systems, Comp. Chem. Eng. 28 (2004) 161–169.
[46] P. Micic, S.N. Bhattacharya, G. Field, Transient elongational viscosity of LLDPE/LDPE blends and its relevance to bubble stability in the film blowing process, Polym. Eng. Sci. 38 (1996) 1685–1693.
[47] W. Minoshima, J.L. White, Instability phenomena in tubular film, and melt spinning of rheologically characterized high density, low density, and linear low density polyethylenes, J. Non-Newtonian Fluid Mech. 19 (1986) 275–302.
[48] J.C. Pirkle Jr., M. Fujiwara, R.D. Braatz, A maximum-likelihood parameter estimation for the thin-shell quasi-Newtonian model for a laboratory blown film extruder, Ind. Eng. Chem. Res. 49 (2010) 8007–8015.

J. Carl Pirkle, Jr. is a senior research associate at the University of Illinois at Urbana-Champaign (UIUC) where he does research in the modeling and systems engineering of chemical processes. After receiving a B.ChE., M.S., and Ph.D. in chemical engineering from the Georgia Institute of Technology, he worked as senior staff at the Applied Physics Laboratory, a postdoctoral fellow in biomedical engineering at John Hopkins University School of Medicine (JHUSM), assistant professor at the JHUSM Department of Biomedical Engineering, head of process modeling at Exxon Research, and director of development and lecturer in the UIUC Department of Chemical Engineering.

Richard D. Braatz is the Edwin R. Gilliland Professor of Chemical Engineering at Massachusetts Institute of Technology where he does research in the modeling, design, and control of chemical, pharmaceutical, and biomedical systems. Honors include the AIChE Excellence in Process Development Research Award, AIChE CAST Outstanding Young Researcher Award, AACC Donald P. Eckman Award, ASEE Curtis W. McGraw Research Award, Antonio Ruberti Young Researcher Prize, Journal of Process Control Prize Paper Award, and Collaboration Success Award from The Council for Chemical Research. He is a Fellow of the Institute of Electrical and Electronics Engineers and the International Federation of Automatic Control.

Please cite this article in press as: J.C. Pirkle Jr., R.D. Braatz, Instabilities and multiplicities in non-isothermal blown film extrusion including the effects of crystallization, J. Process Control (2011), doi:10.1016/j.jprocont.2010.12.007